Absolute cross section of the ^{12}C(p, γ)^{13}N reaction

K-U. Kettner [1,2] H. W. Becker [3] C. R. Brune,[4] R. J. deBoer [2] J. Görres,[2] D. Odell [4] D. Rogalla,[3] and M. Wiescher [2]

[1]*Fachhochschule Bielefeld, 33619 Bielefeld, Germany*

[2]*Department of Physics and Astronomy and the Joint Institute for Nuclear Astrophysics,*
University of Notre Dame, Notre Dame, Indiana 46556, USA

[3]*Rubion, Ruhr Universität Bochum, 44801 Bochum, Germany*

[4]*Institute of Nuclear and Particle Physics and Department of Physics and Astronomy, Ohio University, Athens, Ohio 45701, USA*

Solar neutrino measurements have recently reached a level of sensitivity such that CNO fluxes can now be experimentally determined. While these first measurements are still only sensitive to the higher energy neutrinos resulting from the β^+ decays of ^{15}O produced by the ^{14}N(p, γ)^{15}O reaction, future measurements will work towards detection of neutrinos from the β^+ decay of ^{13}N from the ^{12}C(p, γ)^{13}N reaction. This paper reports on a recent measurement of the ^{12}C(p, γ)^{13}N reaction covering a broad laboratory energy range between 1.0 and 2.5 MeV. The measurement was made to better determine the overall normalization of the absolute cross section and to explore the interference effects between the two broad, overlapping resonances at proton energies of 0.460 and 1.689 MeV and the direct capture to the ground state of ^{13}N in the framework of a multichannel R-matrix analysis. This work takes into account previous radiative capture as well as elastic ^{12}C(p, p)^{12}C scattering data, making uncertainty estimations using a Bayesian framework, to determine a reliable extrapolation of the low energy S factor towards the stellar energy range of CNO hydrogen burning. These new experimental results, and a detailed investigation of the past literature data, suggest that the resonant component of the cross section should be 30% lower than previously accepted.

I. INTRODUCTION

The success of the BOREXINO Collaboration [1] in detecting the first CNO neutrinos from the β^+ decay of ^{15}O produced by the ^{14}N(p, γ)^{15}O reaction, opened up neutrino detection as a direct probe of the metallicity of the solar interior [2,3]. A reliable analysis requires detailed knowledge of the ^{14}N(p, γ)^{15}O reaction rate for the burning conditions in the solar core. It is therefore necessary to know the reaction rate with high accuracy. Most of the reaction rates of solar hydrogen burning rely on the extrapolation of experimental data and thus their accuracy depends critically on the level of knowledge of the contributing reaction components. Such an analysis was recently completed for the ^{14}N(p, γ)^{15}O reaction, summarizing its present status and the associated uncertainties in its reaction rate [4].

The ^{12}C(p, γ)^{13}N reaction determines the strength of the second CNO neutrino source in our sun due to the decay of ^{13}N. Presently the uncertainty of the reaction rate at solar temperature conditions has been evaluated to be about 25%, based on the extrapolation of previous radiative capture studies [5,6]. The neutrinos from the β^+ decay of ^{13}N are emitted with a substantially lower energy than those from ^{15}O decay, which makes their direct detection a formidable task.

The ^{12}C(p, γ)^{13}N reaction, however, also plays an important role in other stellar environments due to the overall large abundance of ^{12}C in our universe. Correlated to the mixing of hydrogen from the hydrogen burning into the helium burning shell of asymptotic giant branch (AGB) stars, it influences the production of ^{13}N, which subsequently decays to ^{13}C triggering the ^{13}C(α, n)^{16}O reaction. The amount of ^{13}C is crucial as the ^{13}C(α, n)^{16}O reaction is the main neutron source for the s [7] and i processes [8], depending on the convection conditions in the helium burning shell.

Finally, it has been argued that the ^{12}C(p, γ)^{13}N reaction also plays an important role in the energy production of a type Ia supernova detonation. The emerging shock front from the ^{12}C + ^{12}C driven ignition raises the temperature of the He accreting shell of the white dwarf [9]. This causes the rapid production of protons by converting ^{14}N, the ashes of the preceding hydrogen burning phase, via the reaction sequence ^{14}N(α, γ)^{18}F(α, p)^{21}Ne [10], releasing free protons that can be captured back onto the existing ^{12}C material at higher temperatures. This sequence may also play an important role in the recently discussed helium detonations at the surface of a white dwarf star in a double-detonation type Ia supernova [11]. Either scenario for type Ia explosions will lead to enhanced temperatures at which the ^{12}C(p, γ)^{13}N reaction may play an important role. The reaction will generate a neutrino signal associated with the ignition. The neutrino flux will depend not only on the explosive environment but also on the actual ^{13}N production rate. While previous derivations of the ^{12}C(p, γ)^{13}N reaction rate have focused on the low energy component, important for stellar CNO hydrogen burning, the data presented here cover a broader range of the excitation curve, also addressing the impact of the reaction in higher

temperature environments. A comprehensive *R*-matrix analysis was thus performed here, which includes not only the ^{12}C(p, γ)^{13}N radiative capture data but also ^{12}C(p, p)^{12}C elastic scattering data to allow for a reliable extrapolation of the reaction cross section.

The following chapters will provide information about the past experimental achievements in studying this reaction and the discrepancies in the experimental results (Sec. II) before turning to the present experiment aimed at identifying and correcting these discrepancies (Sec. III). This will be followed by a description of the experimental setup and the analysis of the cross section data (Sec. IV) before the *R*-matrix and Bayesian uncertainty analysis (Sec. V) that demonstrates the level of consistency between present and past data sets is discussed (Sec. VI). From this, a revised reaction rate is derived for a wide temperature range (Sec. VII) and a final summery is made (Sec. VIII).

II. PREVIOUS EXPERIMENTAL RESULTS

At the beginning of 1934, Joliot and Curie published their seminal paper on the detection of artificial radioactivity [12] from ^{13}N, ^{27}Si, and ^{30}P, by bombarding the elements boron, magnesium, and aluminum with α particles from a polonium source. They also suggested that ^{13}N could be produced by the interactions of protons and deuterons with carbon. In the following year, Joliot and Curie received the Nobel Prize in Chemistry for this achievement [13].

Following the suggestions of Joliet and Curie, the first ^{12}C(p, γ)^{13}N activation studies were performed by Cockcroft *et al.* [14] and Hafstad and Tuve [15] in 1935 and Roberts and Heydenburg [16] in 1938 by way of the produced radioactivity. The first radiative capture measurements, detecting the emitted γ-ray radiation directly, were performed by Curran *et al.* [17] in 1938 and then by Tangen [18] during the Second World War in German occupied Norway.

After the war, a large number of proton capture experiments on ^{12}C were performed, which are summarized in the compilations of Ajzenberg-Selove and Lauritsen [19] and Ajzenberg-Selove [20]. With the identification of the CNO cycles as an important process by Bethe and Weizsäcker in 1936 [21] the relevance of the ^{12}C(p, γ)^{13}N reaction shifted from being one of the early examples of nuclear transmutation to one of the key reactions in the CNO cycles. This recognition triggered a new era of experimental activities in the late 1940s, namely in the low energy range of the reaction, which would characterize the reaction rate in stellar environments [22,23]. These were followed by more extensive studies using thick and thin ^{12}C targets, used for mapping the reaction over a wider laboratory proton energy range from $E_p = 0.4$ to 2.6 MeV, identifying several broad and overlapping resonances [24,25].

Similar studies turned to measurements of the low-energy resonance at $E_p = 460$ keV and its low energy tail that extends into the stellar energy regime. Some of them relied on the activation approach such as those of Hall and Fowler [26] and Bailey and Stratton [27], while others focused on the measurement of the γ-ray radiation associated with the ground state transition [28–30]. All of these studies relied on

the thick-target technique, but used different stopping powers to convert the yield data into cross sections. Another attempt was pursued by Young *et al.* [31] who studied the reaction cross section towards higher energies between $E_p = 1.5$ and 2.0 MeV to investigate the impact of possible interferences between the resonances. This was followed by the work of Rolfs and Azuma [32], who measured the reaction over a broad energy range from $E_p = 0.15$ to 2.5 MeV and performed an extensive analysis of the interference structure of the cross section using a potential model for the direct capture and a Breit-Wigner analysis for the resonance contributions. A first *R*-matrix analysis of the low energy cross section data was performed by Barker and Ferdous [33] using a single-channel, multilevel, code. This was followed up by similar analyses by Hinds and Barker [34], Li *et al.* [35], and Artemov *et al.* [36], whereas Burtebaev *et al.* [37] and NACRE II [5] used a potential model. A multichannel, mult-level, analysis has also been performed using the code AZURE [6], which also simultaneously fits ^{12}C(p, p)^{12}C data [38].

The comparison of the different data sets, however, reveals a number of inconsistencies that make a straight forward comparison and analysis over a wide energy range in terms of *R*-matrix theory impossible. This has primarily to do with the differences in the stopping powers used to determine the energy loss and resolution effects for the low energy protons in the carbon targets. This is a result of the substantial changes in the tabulated stopping powers that occurred over the years due to the development of stopping power theory, but there may also be other experiment based reasons. One important goal of this work is therefore to provide a revised normalization for the cross section data based on past data sets, and the new data presented in this study that will resolve the existing discrepancies and uncertainties.

III. EXPERIMENTAL SETUP

Several experimental measurements were performed at both the University of Notre Dame and the University of Bochum. The measurements at the University of Notre Dame centered around thin-target excitation function and angular distribution measurements from $E_p = 1$ to 2.5 MeV and thick-target yield measurements from $E_p = 1$ to 2 MeV. The measurements at the University of Bochum were made using thin targets on the $E_p = 460$ keV resonance in the ^{12}C(p, γ)^{13}N reaction in order to characterize the targets and confirm the absolute cross section at this resonance energy. The experimental setups are described here while experimental descriptions and data analysis are described in Sec. IV.

A. University of Notre Dame

Excitation function and angular distribution measurements of the ^{12}C(p, γ)^{13}N reaction were performed at the 4-MeV KN Van de Graaff accelerator at the University of Notre Dame Nuclear Science Laboratory. The accelerator provided proton beams over an energy range from $E_p = 1.0$ to 2.5 MeV, with beam intensities of up to 150 µA on target. The energy calibration of the acceleration system was performed, determining the beam energy with an accuracy of ± 1 keV using the well
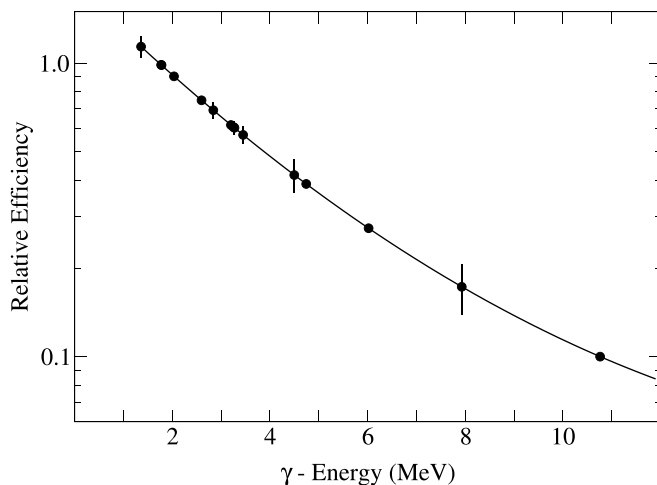
FIG. 1. The efficiency of the experimental setup for a detector located at 55° based on the decay lines of a ^{56}Co source and the γ transitions of the ^{27}Al$(p, \gamma)^{28}$Si resonance at $E_p = 992$ keV, measured at a distance of 259 mm between target and detector.

know resonances of the ^{27}Al$(p, \gamma)^{28}$Si reaction at $E_p = 0.992$ and 1.8 MeV [39].

A single, high resolution, 55% relative efficiency, high-purity germanium (HPGe) detector was positioned at two distances from the target for measurements in far (259 mm) and close (61 mm) geometry between the detector and the water-cooled target. For angular distribution measurements, the detector was rotated around the target with an accuracy of 1° in the near geometry position. The beam was swept horizontally and vertically across a target area of 1 cm^2 in order to dissipate power over a larger target area. To minimize the buildup of additional carbon on the target, a liquid nitrogen cooled copper pipe was mounted inside the beam line, extending as close to the target as possible. In addition, a bias voltage of -400 V was applied to the isolated cold finger to suppress the secondary electrons ejected from the target during beam bombardment.

The energies of the γ-ray transitions of interest ranged from $E_\gamma = 2900$ to 4300 keV. The front surface of the HPGe detector was covered with a 3 mm lead sheet to reduce the intensity of low energy γ-ray radiation background. The efficiency of the γ-ray detection in this arrangement was measured using a radioactive ^{56}Co source along with the γ-ray transitions from the well-known ^{27}Al$(p, \gamma)^{28}$Si resonance at 992 keV [39] as shown on Fig. 1. The efficiency measurements were performed independently for each of the distances and angle positions of the detector.

B. University of Bocham

Target fabrication and characterization was performed at the RUBION facility at the University of Bocham [40]. γ-rays were detected with a large volume HPGe detector with a nominal relative efficiency of 100%. The detector was placed at 0° relative to the beam axis. The γ rays at the $E_p = 460$ keV resonance in the ^{12}C$(p, \gamma)^{13}$N reaction were isotropic as were the reference γ rays from the $E_p = 278$ keV resonance in the

^{14}N$(p, \gamma)^{15}$O reaction. The efficiency of the detector was determined using calibrated ^{152}Eu and ^{60}Co sources with 2σ uncertainties of 1.3% and 1.0%, respectively. The source measurements were extended to higher energies using the well known γ-ray decay scheme of the $E_p = 278$ keV resonance in the ^{14}N$(p, \gamma)^{15}$O reaction, where its resonance strength was 12.6(3) meV [41]. The primary transition to the 5.18 MeV bound state, with a branching ratio of 16.9(4)%, had a γ-ray energy that was within 2 keV of that of the ground state transition from the ^{12}C$(p, \gamma)^{13}$N reaction at the $E_p = 460$ keV resonance. The target and chamber were electrically isolated and a liquid nitrogen cooled Cu shroud extended to within 5 mm of the target surface. The shroud was biased to -300 V to suppress secondary electrons. In addition, strong permanent magnets were placed at the gap between target and shroud for additional suppression.

The calibration measurements were done with detectors at two positions, a near position at a distance of 15 mm between the target and the front face of the detector and a far position at a distance of 253 mm. The near position was used to measure yields over the $E_p = 460$ keV resonance in the ^{12}C$(p, \gamma)^{13}$N reaction. The far position was used for the relative strength measurements using the ^{14}N$(p, \gamma)^{15}$O reaction and calibrated sources. At this distance, summing corrections were negligible. Repeated scans were performed to characterize uncertainties from sources such as charge collection, target stability, and beam positioning on the target. For the final setup, yield reproducibility at the $\approx$1% level was achieved.

C. Targets

The isotopically enriched carbon targets were produced by implantation at the Dynamitron Tandem Laboratory at the University of Bochum by bombarding 0.5 mm backings of tungsten or tantalum with a 80 μA ^{12}C beam at either 30 or 50 keV over an area of 3.14 cm^2. For the higher energy measurements at the University of Notre Dame, an implantation energy of 50 keV and a tungsten backing were used, while, for the measurements at the $E_p = 460$ keV resonance performed at the University of Bochum, an implantation energy of 30 keV and tantalum were used. Different implantation energies were used so that the energy losses of the beam for the two measurements were similar. For the 50 keV implantation energy targets, a total of 0.73 C was deposited resulting in an estimated 1.4×10^{18} carbon atoms/cm^2, while for the 30 keV targets the charge deposited was 0.52 C leading to 1.0×10^{18} carbon atoms/cm^2. The actual number of implanted ions was somewhat lower since the implantation process has an efficiency that is less than 100% (see Sec. IV C).

For the measurements at the University of Notre Dame, the relative target thickness was monitored by the γ-ray peak shape of the direct capture or broad resonance related primary γ-ray transition, which exhibited both the energy resolution of the accelerator and detector as well as the energy loss through the target. At a beam energy of $E_p = 1700$ keV, the beam energy loss was found to be $\Delta E = 14$ keV. The stability of the target was continuously checked by monitoring the ^{12}C$(p, \gamma)^{13}$N spectrum at this same energy. A gradual linear

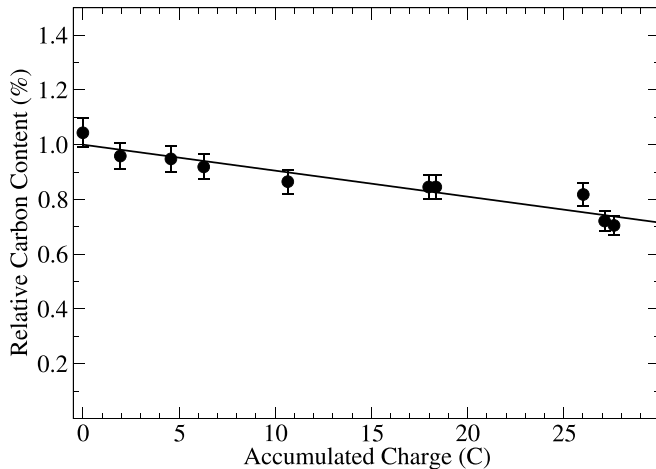FIG. 2. All ^{12}C(p, γ)^{13}N measurements were acquired with the same target. Ten stability checks were performed over the course of the experiments by making repeated measurements at $E_p = 1700$ keV to monitor target degradation. A linear degradation was found as a function of deposited charge. The total loss after two weeks and a median current of about 100 μA was less ≈30%.

deterioration was observed over the course of the experiment, resulting in a total accumulated charge of 27 C, which was corrected assuming a linear dependence of target thickness deterioration with charge as shown in Fig. 2. After two weeks of running, with a median current of about 100 μA, a total loss of ≈30% of the thick target was recorded.

IV. EXPERIMENT AND DATA ANALYSIS

The three experimental campaigns described in this section provided a consistent set of data to which all existing ^{12}C(p, γ)^{13}N data could be renormalized. The thin-target data from the present measurements can be found in tabular form in the Supplemental Material [42].

A. Excitation functions and angular distribution measurements

At the University of Notre Dame, an excitation curve of the ^{12}C(p, γ)^{13}N reaction was measured in small, well calibrated energy steps between $E_p = 1.0$ and 2.5 MeV at 0 and 55° to expand the existing data range of the reaction towards higher energies and to study the interference patterns in this energy range. Figure 3 shows the ^{12}C(p, γ)^{13}N ground state transition in the γ-ray spectrum at three different energies, demonstrating the energy shift of the emitted γ-ray radiation with beam energy. The excitation curves are shown in Fig. 4.

In addition to the excitation curves, angular distribution data were taken in 100 keV steps between $E_p = 1.2$ and 2.49 MeV as shown in Fig. 5. The goal was to obtain an extended data set for a more reliable R-matrix analysis of the reaction mechanisms and the associated interference effects, complementing previous low energy angular distribution results towards the higher energy range. By comparing with the well known angular distributions from the transitions in the ^{27}Al(p, γ)^{28}Si reaction [39], the geometric Q coefficients [43] were determined to correct for the extended geometry
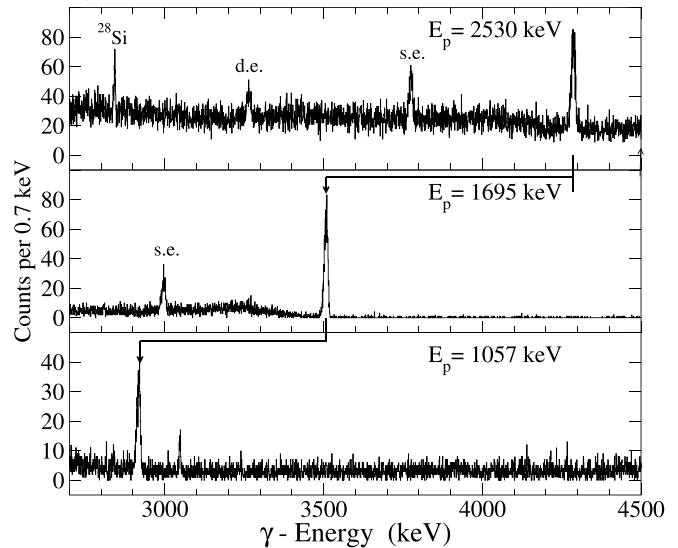

FIG. 3. The γ-ray spectrum from the ^{12}C(p, γ)^{13}N reaction at three different proton beam energies. The shift in γ-ray energy with the beam energy clearly demonstrates a mechanism based on the broad resonance at $E_p = 1.6$ MeV interfering with the underlying direct capture population of the ground state. Single escape (s.e.) and double escape (d.e.) peaks are indicated.

of the detector when comparing with theory calculations. The coefficients are given in Table I.

B. Thick-target activation measurement

A second experiment was performed at the University of Notre Dame based on the activation technique, which determined the thick-target yield of the ^{12}C(p, γ)^{14}N reaction by measuring the β^+ decay curve of the ^{13}N produced during irradiation by way of the intensity of the 511 keV

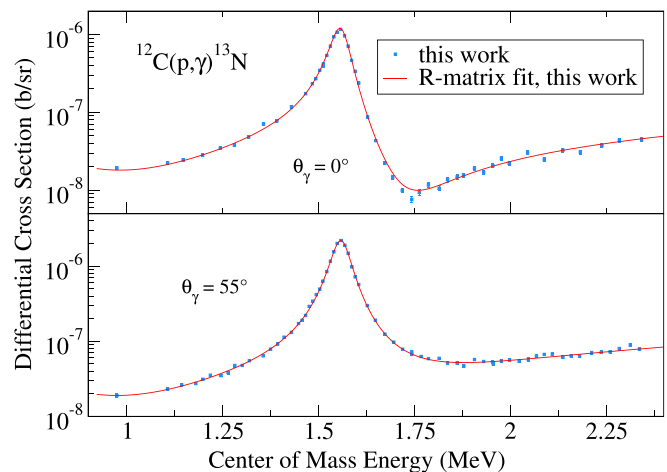

FIG. 4. Excitation functions of the ^{12}C(p, γ)^{13}N reaction at $\theta_\gamma = 0$ and 55° compared to the R-matrix fit described in Sec V. Note that the absolute cross section of the excitation functions was obtained by normalizing to the R-matrix cross section, whose scale is constrained by the lower energy data.
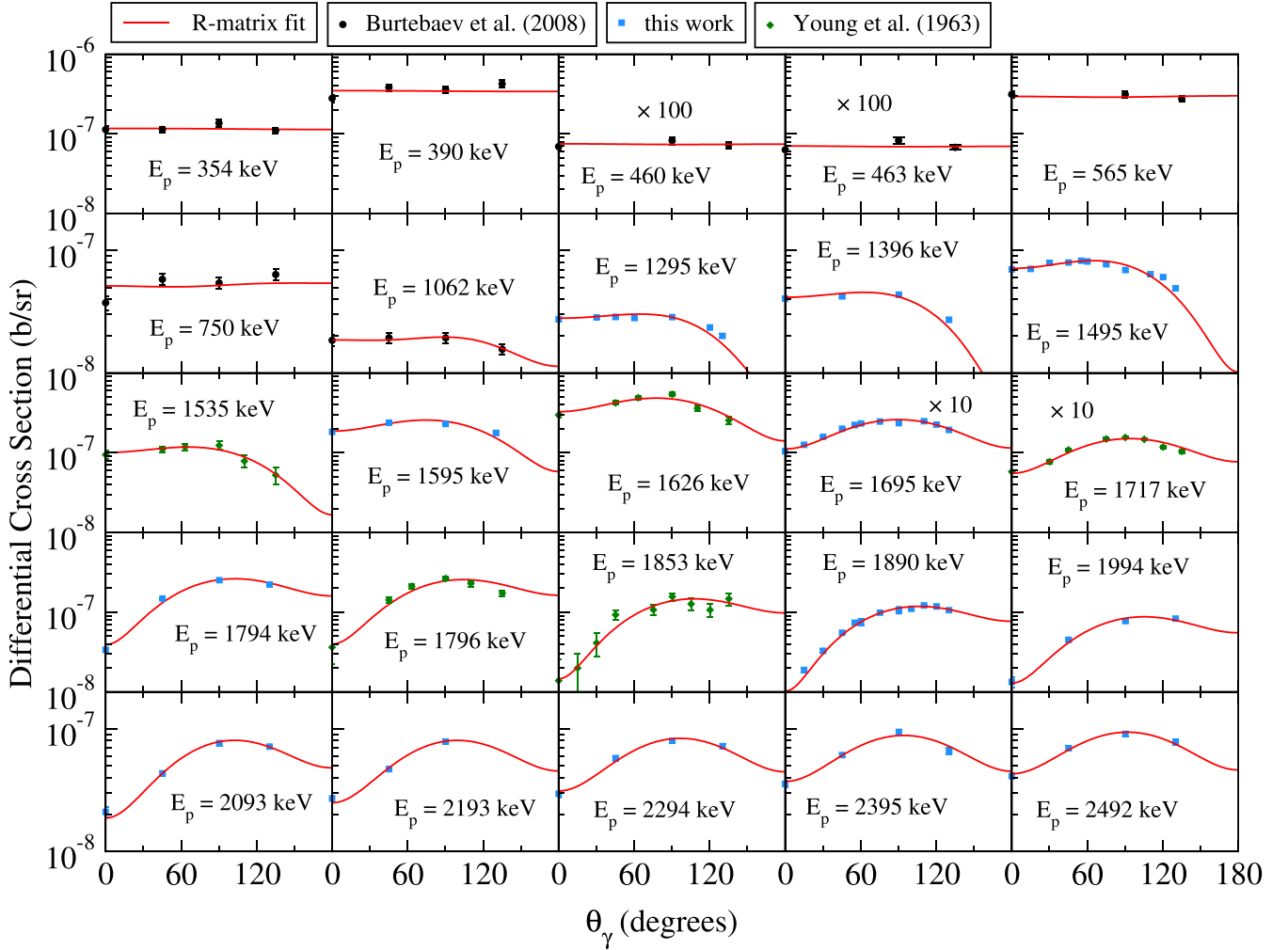
FIG. 5. Angular distributions of the $^{12}\text{C}(p, \gamma)\,^{13}\text{N}$ reaction of this work (blue squares) compared to the previous work of Burtebaev *et al.* [37] (black circles) and Young *et al.* [31] (green diamonds) and the *R*-matrix fit described in Sec. V. Where indicated, the cross section scale should be multiplied by the indicated factor. Note that the absolute cross section for the angular distributions was obtained by normalizing to the *R*-matrix cross section.

annihilation γ-ray line. The target was a 0.02 in. thick graphite sheet, thick enough to completely stop the proton beam, which was irradiated for 20 minutes with beam intensities ranging between 0.7 and 2.5 μA. Afterwards, the target was moved to a lead-shielded, low background counting station and positioned 10 cm in front of a 124% relative efficiency HPGe detector. The average transport time was 3.5 minutes between target and counting station. Typically, the 511 keV decay line was measured once per minute for 30 minutes. In two cases, at $E_p = 1.2$ and 1.4 MeV, the counting time was doubled to

TABLE I. Relative geometric Q coefficients for the present work and that of Burtebaev *et al.* [37].

	This work	Burtebaev *et al.* [37]
Q_1	0.943	0.95
Q_2	0.834	0.83
Q_3	0.688	
Q_4	0.517	

60 minutes to achieve better comparison with the data of Seagrave [24]. A calibrated ^{22}Na source was used to determine the efficiency of the counting arrangement.

The activation runs were performed at five energies between $E_p = 1$ and 2 MeV to obtain the activation yields that have dominant components from both the lowest energy $E_p = 460$ keV resonance and the next highest at $E_p = 1690$ keV in the $^{12}\text{C}(p, \gamma)\,^{13}\text{N}$ reaction. Figure 6 shows a typical decay curve for the ^{13}N activity of the target after irradiation at $E_p = 1.2$ MeV. The observed half-life of $T_{1/2} = 9.928(38)$ min agreed well with the compilation value of $T_{1/2} = 9.965(4)$ min [44], which demonstrated that no other decay products of appreciable strength had been generated as background during the experiment. The reaction yield per incoming proton obtained through the fit of the activation curves for the different irradiation energies is given in Table II.

The activation yield corresponds to the thick-target yield of a radiative capture measurement at the corresponding energies. While several energies were taken, the thick-target yield from the activation runs at $E_p = 1$ and 2 MeV were utilized
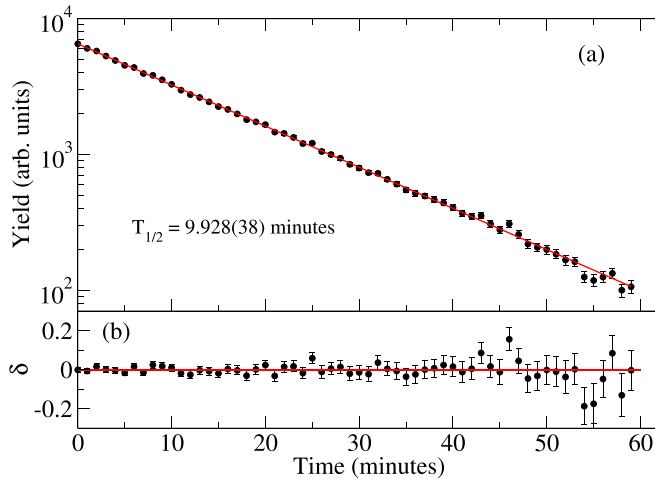
FIG. 6. (a) 511 keV γ-ray yield observed after activation of the thick ^{12}C target, sampled once per minute. The data were well reproduced, as shown by the residual plot (b), by a single decay curve, yielding a half-life for ^{13}N of 9.928(38) minutes, in good agreement with the accepted value of 9.965(4) minutes [44].

to extract the difference in the yield as a function of energy, since the integral from zero energy to the beam energy of the activation scales directly to the measured yield resulting from the resonance cross section. The $E_p = 1$ MeV yield results from the on-resonant cross section of the $E_p = 460$ keV resonance and was found to correspond to 100(6) μb, as discussed further in Sec. IV D. The $E_p = 2$ MeV yield (minus the $E_p = 1$ MeV yield) can be used to calculate the cross section of the $E_p = 1.69$ MeV resonance. These thick-target yields are in excellent agreement with the results of Seagrave [24] when the systematic uncertainty of that work is considered. The thick-target measurements from an unpublished work by Fowler, Seagrave [24], Hinds and Barker [34], and the present work are compared in Fig. 7.

C. Target characterization and $E_p = 460$ keV cross section measurements

A third set of experiments were performed at the RUBION facility at the University of Bochum. The number of target atoms was deduced using two independent methods with two different carbon targets using experimental setups on the 4 MeV Tandem Accelerator. The first method used Nuclear Reaction Analysis using a deuteron beam (D-NRA).

TABLE II. The thick-target reaction yield per incoming particle extracted from the activation data for the different irradiation energies. The overall systematic uncertainty is 2.5%.

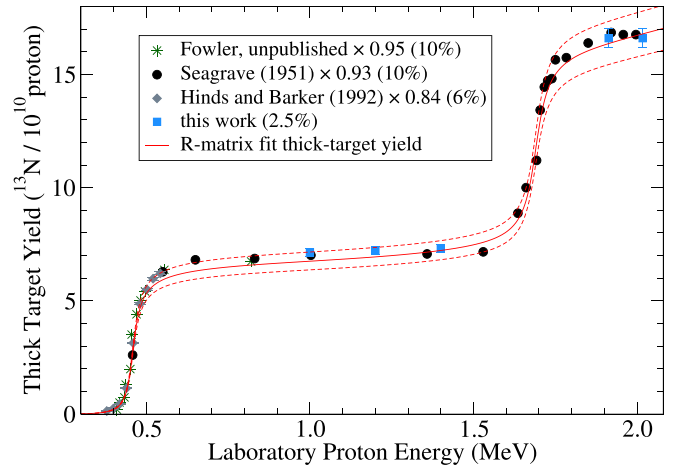| E_p (MeV)	Yield per incoming proton
1.000(1)	$7.14(14) \times 10^{-10}$
1.200(1)	$7.22(14) \times 10^{-10}$
1.400(1)	$7.31(15) \times 10^{-10}$
1.913(1)	$1.66(3) \times 10^{-9}$
2.017(1)	$1.66(3) \times 10^{-9}$

FIG. 7. Comparison of thick-target yield measurements from an unpublished work by Fowler (which is given in Seagrave [24]), Seagrave [24], Hinds and Barker [34], and the present work. The experimental values are compared with the integrated cross section of the *R*-matrix fit described in Sec. V, where the uncertainty band for the *R*-matrix calculation corresponds to the uncertainty in the SRIM stopping power. Except for the data of Hinds and Barker [34], the absolute scale of the previous data agrees well with the present work when their systematic uncertainties are considered. To better facilitate comparison, the yields of the data sets are scaled by a multiplicative factor as indicated. All of the data have a consistent energy dependence.

This method utilized the well known ^{12}C(d, p_0) ^{13}C reaction at a laboratory deuteron energy of 1 MeV where the cross section was slowly varying in energy [45,46]. The second method used Rutherford backscattering (RBS), where 2 MeV α particles were used. The target thickness determined using both methods agreed to within 5%, giving a value of $6.30(49) \times 10^{17}$ atoms/cm^2. The $E_p = 460$ keV on-resonance cross section of the ^{12}C(p, γ) ^{13}N reaction was also determined relative to the resonance strength of the ^{14}N(p, γ) ^{15}O reaction at the $E_p = 278$ keV resonance [41,47] using the 500 kV accelerator. The γ-ray transitions of both resonances were isotropic and the energy of the transition to the 5.18 MeV state in ^{15}O was the same (within 1–2 keV) as that of the ^{12}C(p, γ_0) ^{13}N reaction. This resulted in an on-resonance cross section of 101(8) μb.

D. Absolute cross section determination

One of the main results of the present work was the realization that the previously reported cross sections of Seagrave [24], Vogl [30], and Rolfs and Azuma [32] were overestimated because of inaccurate stopping powers used originally by Seagrave [24]. While it was not emphasized, Vogl [30] did not make an absolute measurement but instead normalized their data to the ground state γ-ray width of the state corresponding to the $E_p = 460$ keV resonance determined previously by Seagrave [24]. Similarly, Rolfs and Azuma [32] normalized their data to that of Vogl [30], seemingly not realizing that Vogl [30] had not made an absolute measurement. These normalization issues were also discussed in Barker and Ferdous [33]

and Hinds and Barker [34], where the absolute normalization of the data presented in the latter paper is consistent with that of this work. The data of Burtebaev *et al.* [37] give an overall cross section scale similar to the older measurements, but, since these measurements were absolute and should have utilized modern stopping powers, the reason for their larger cross section was unclear.

This difference in the cross section was found in the present work by comparing the absolute thick-target yields of this work with that of Seagrave [24], which were in good agreement, yet the absolute thin-target cross sections of Vogl [30] were $\approx 30\%$ larger in absolute cross section compared to the present measurements. The only significant source of uncertainty in the conversion from thick-target yield to cross section was the stopping power of protons in carbon. The stopping power used by Seagrave [24] can be found in their thesis [48], and, at the energy of the $E_p = 460$ keV resonance in the ^{12}C$(p, \gamma)^{13}$N reaction, their stopping power was $\approx 30\%$ smaller than the modern stopping power found in SRIM [49]. Using the modern stopping power and the thick-target yield data of this work gives an absolute cross section of 100(6) μb at the peak of the $E_p = 460$ keV resonance, compared to the value of 127 μb used by Refs. [24,25,30,32].

The absolute cross section and uncertainty were obtained from the activation measurement described in Sec. III and the modern stopping power from SRIM [49] as described in Sec. IV B. The cross section was also determined independently relative to the strength of the $E_p = 278$ keV resonance in the ^{14}N$(p, \gamma)^{15}$O reaction at the $E_p = 460$ keV resonance in the ^{12}C$(p, \gamma)^{13}$N reaction, where a consistent value of 101(8) μb was obtained IV C. The uncertainty in the thick-target yield measurements is 2.5%, with uncertainties coming from the accuracy of the charge reading (2%), the γ-ray detection efficiency at 511 keV (1%, as determined with a calibrated ^{22}Na source), and statistics ($< 1\%$). From the present SRIM evaluation, the estimated uncertainty in the stopping power is $\approx 5\%$ over the energy range of the present measurements and those of Seagrave [24]. Therefore, a total uncertainty in the ^{12}C$(p, \gamma)^{13}$N cross section of 6% is adopted.

V. *R*-MATRIX AND BAYESIAN UNCERTAINTY ANALYSIS

The simultaneous *R*-matrix analysis of the ^{12}C$(p, \gamma)^{13}$N and ^{12}C$(p, p)^{12}$C reactions was performed using the code AZURE2 [6,50]. The analysis utilized the alternative *R*-matrix parametrization of Brune [51] in order to directly compare with observable level parameters from the literature. This analysis represents a continuation of that presented in Azuma *et al.* [6], where the capture cross section data have now been expanded to include the present data and those of Burtebaev *et al.* [37] and Young *et al.* [31]. The same channel radius of 3.4 fm was used. Masses and separation energies were taken from the AME 2016 mass evaluation [52,53]. Angular resolution effects in the differential cross section data of the present work and those of Burtebaev *et al.* [37] were taken into account using the *Q* coefficients given in Table I.

Three resonances ($E_{c.m.} = 425$, 1558, and 1601 keV) were required to accurately describe the experimental scattering
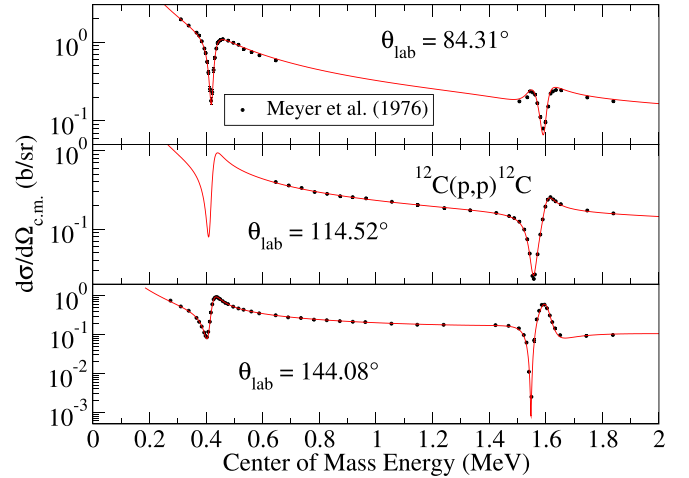

FIG. 8. Comparison of the ^{12}C$(p, p)^{12}$C data of Meyer *et al.* [38] with the *R*-matrix fit of the present work.

data of Meyer *et al.* [38], which correspond to the well known levels in the ^{13}N system at $E_x = 2.36\,(1/2^+)$, $3.50\,(3/2^-)$, and $3.55\,(5/2^+)$ MeV ($S_p = 1.9435(3)$ MeV [52,53]) as shown in Fig. 8. Because their widths were large (≈ 60 and 50 keV, respectively) compared to their level spacing, the resonances that correspond to the 3.50 and 3.55 MeV levels appeared as an unresolved doublet. The fitting of the accurate and precise thin-target data of Meyer *et al.* [38] placed strong constraints on the energies and proton partial widths of these levels, two of which, those at $E_x = 2.36$ and 3.50 MeV, corresponded to the two strong resonances observed in the radiative capture reaction.

There are many other elastic scattering data sets available in the literature, but they generally use significantly thicker targets, where the *R*-matrix cross section would have to be convoluted with the experimental resolutions. This introduces another source of uncertainty that would add further complexity to the fitting and uncertainty propagation. It is for this reason that only the scattering data of Meyer *et al.* [38] are considered.

With the *R*-matrix fit to the scattering data providing tight constraints on the energies and proton widths, the fitting of the radiative capture data is simplified as the only additional free parameters are the γ-ray partial widths. As discussed in Sec. II, there are surprisingly few low-energy studies of the ^{12}C$(p, \gamma)^{13}$N reaction; however, many of them have very little distortion to their reported cross sections, as thin, robust carbon targets are easily fabricated. Further, the energy dependence of many of the measurements are in very good agreement, as will be discussed further in Sec. VI.

The data of Vogl [30] report high energy resolution angle integrated cross section data measured over the lowest energy resonance ($178 < E_{c.m.} < 630$ keV) in fine energy step spacing. The angular distribution data of Young *et al.* [31] have been included as they provide a good comparison for the present measurements, being made over a similar energy ($1417 < E_{c.m.} < 1710$ keV) range. The angle integrated data of Hinds and Barker [34] are limited to the peak region of the lowest energy resonance. The most recent experimental data
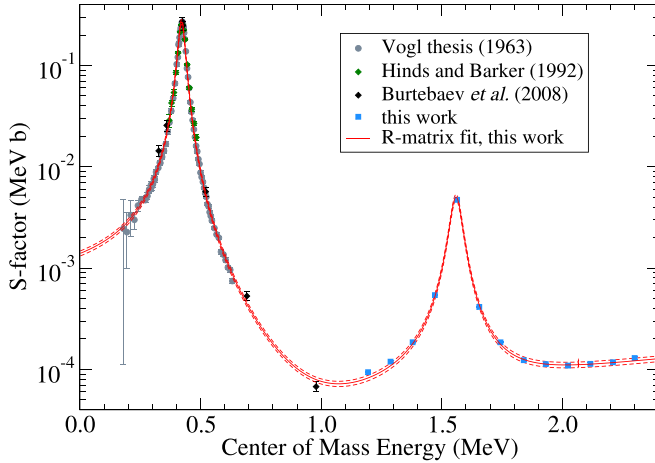
FIG. 9. Comparison of the angle integrated ^{12}C(p, γ)^{13}N radiative capture S factors for the data of [30], Hinds and Barker [34] and Burtebaev *et al.* [37] (renormalized as discussed in the text). The angle integrated S factor from the present data, obtained by a Legendre fit to the measured angular distributions, is also shown for comparison. The solid red line represents the best R-matrix fit while the dashed red lines indicate the 68% confidence interval obtained from the Bayesian uncertainty analysis using the BRICK code [54].
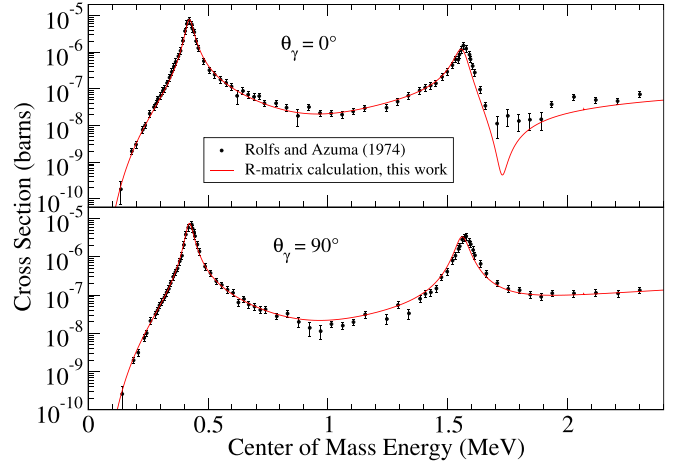

FIG. 10. Comparison of the present R-matrix fit with the data of Rolfs and Azuma [32], renormalized as discussed in the text. The data were not included in the present fit because of a discrepancy with their energy calibration above ≈ 1 MeV.

are those of Burtebaev *et al.* [37], who report both angular distributions and an absolute angle integrated cross section over the lowest energy resonance ($327 < E_{\text{c.m.}} < 979$ keV). Finally, the differential cross section data of the present work span the energy range from $976 < E_{\text{c.m.}} < 2338$ keV with angles of measurement at $\theta_\gamma = 0$ and $55°$. Angular distributions are given at several energies with between 4 and 11 angles of observation. These data are compared with the R-matrix fit in Figs. 4, 5, and 9.

The R-matrix fit to the radiative capture data requires three main types of reaction components. First, there are two clear resonances that come from primarily $E1$ and $M1$ decays from the $E_x = 2.36$ and 3.50 MeV levels in ^{13}N, respectively. While deexcitation from the $E_x = 3.55$ MeV state is possible via $M2$ or $E3$ multipolarities, there is no experimental evidence for this at the sensitivity of the present measurements. While the γ-ray decay of the $E_x = 3.50$ MeV resonance is dominated by $M1$ multipolarity, a small $E2$ component is statistically significant in the fit. This is discussed further in Sec. VI. The second component is external capture, which is used to model the hard sphere component of the direct capture process [55–57]. In the case of the ^{12}C(p, γ_0)^{13}N reaction, $E1$ multipolarity dominates but the weaker $E2$ contribution is found to have a small but significant interference contribution. The third components are those of background levels of $J^\pi = 1/2^+$ $(E1)$ and $3/2^-$ $(M1/E2)$. The background components are only necessary in order to fit the highest energy data above $E_{\text{c.m.}} \approx 1.75$ MeV.

The R-matrix fit was first performed using the least-squares routine built into AZURE2, as a first step in finding the optimum fit parameters. These parameters were then used as starting values for the Bayesian R-Matrix Inference Code Kit (BRICK) [54] to perform a Markov chain Monte Carlo (MCMC) uncertainty estimation using the EMCEE [58]

package. The R-matrix fit parameters and data set normalization factors were given uniform prior probability density functions (PDFs), except for the data set of Vogl [30]. These data were renormalized to a 100 μb cross section at the $E_p = 460$ keV resonance and their absolute normalization was given a Gaussian prior PDF equal to the systematic uncertainty of 6% discussed in Sec. IV D. The best fit was then taken as the 50% quantile of the resulting posterior distributions for each fit parameter and the uncertainties were determined from the 16% and 84% quantiles. As all of the parameters needed for the fit were well constrained by the experimental data, the posterior PDFs were all well described by a Gaussian distribution. In addition, the MCMC routine provided a straightforward way of calculating the uncertainties in the R-matrix cross sections and S factors. The best fit parameters and their uncertainties are given in Table III.

VI. DISCUSSION

In the R-matrix fit and Bayesian uncertainty analysis presented in Sec. V, the data sets of Hall and Fowler [26], Bailey and Stratton [27], Lamb and Hester [28], and Rolfs and Azuma [32] were not included because of inconsistencies with these data sets and incomplete uncertainty information. Differential cross sections at $\theta_\gamma = 0$ and $90°$ were reported by Rolfs and Azuma [32] spanning a wide energy range ($138 < E_{\text{c.m.}} < 2308$ keV). However, the energy calibration of this data was inconsistent with other measurements. Further, the energy miscalibration was difficult to correct because the data were measured at two different facilities, each with different energy calibrations, and the division of the data was not indicated. For this reason this data were not included in the R-matrix fit, but a comparison of the data with the fit is shown in Fig. 10. In Rolfs and Azuma [32], it was found that the angular distributions were of sufficient precision to place a constraint on the $M1/E2$ multipole mixing ratio of the $E_x = 3.50$ MeV level in ^{13}N, which corresponds to the

TABLE III. R-matrix parameters resulting from a Bayesian MCMC analysis to $^{12}C+p$ data. The central values represent 50% quantiles of the posterior PDFs while the uncertainties correspond to the 16% and 85% quantiles. The posterior PDFs closely resemble a Gaussian distribution. Note that the uncertainty in the excitation energies are of the form (MCMC + systematic), where the 0.5 keV (laboratory frame) systematic uncertainty of Meyer *et al.* [38] was not included in the MCMC analysis. The sign of a partial width indicates the sign of the corresponding reduced width amplitude.

E_p (keV)	E_x (MeV)		J^π	Γ_p (keV) or ANC (fm$^{-1/2}$)		Γ_{γ_0} (eV)	
This work	This work	Ref. [44]	Ref. [44]	This work	Ref. [44]	This work	Ref. [44]
	0.0	0.0	$1/2^-$	1.62(5)			
460.3(5)	2.3682(1+46)	2.3649(6)	$1/2^+$	34.0(2)	31.7(8)	−0.48(3)	0.50(4)
1688.8(5)	3.5032(1+46)	3.502(2)	$3/2^-$	55.2(3)	62(4)	$0.49(3)/7.2(11) \times 10^{-4}$ [a]	0.64
1735.5(5)	3.5453(2+46)	3.547(4)	$5/2^+$	49.0(5)	47(7)		
	Background levels						
	20[b]		$1/2^+$	5×10^4 [b]		$5.4(5) \times 10^3$	
	20[b]		$3/2^-$	5×10^4 [b]		$-120(20)/1.1(2) \times 10^3$ [a]	

[a]$M1/E2$.
[b]Fixed parameter.

resonance observed at $E_p = 1689$ keV. In the present work a value of $\delta = 0.038(6)$ was found, while Rolfs and Azuma [32] found a significantly larger value of 0.09(2). The reason for this discrepancy is unclear.

In the 1950s several very low energy measurements of the $^{12}C(p,\gamma)^{13}N$ cross section were undertaken using thick-target techniques and very high (milliampere) beam intensities [26–28]. The cross sections deduced from these thick-target measurements were compared with the present fit and the lowest energy data of Vogl [30] in Fig. 11. While the mean value of these data were found to be in generally good agreement with the extrapolated S factor of this work, it was clear from the large scatter of the data that the uncertainties were underestimated. Thus these data were not included in the present analysis.
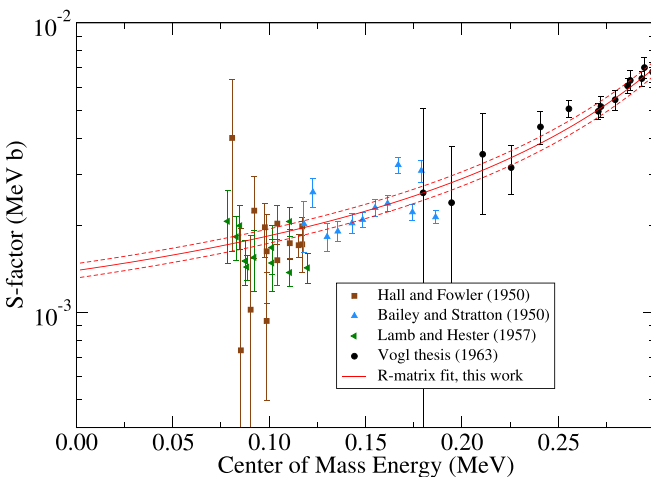

FIG. 11. Comparison of the extrapolated R-matrix fit and uncertainty from the analysis described in Sec. V, where the bands correspond to a 68% confidence level, with the low energy data of Hall and Fowler [26], Bailey and Stratton [27], and Lamb and Hester [28], with no adjusted normalization. The lowest energy data of Vogl [30], renormalized as described in the text, are also shown for comparison.

To test the sensitivity of the low energy extrapolation of the S factor to the new measurements reported in this work, the R-matrix fit and Bayesian analysis was repeated in its absence, thus without any higher energy data. It was found that this higher energy data had little direct effect on the uncertainty in the low energy extrapolation, as the data of Vogl [30] and Burtebaev *et al.* [37] map a wide enough region of the off-resonance tail of the $E_p = 460$ keV resonance to also constrain the magnitude of the direct capture contribution. However, this uncertainty calculation in the extrapolation was made using only the R-matrix components that were statistically necessary in order to fit the experimental data; that is, there could be weak background components that effected the extrapolated S factor but had very little affect on the fitting of over the energy range of the experimental data. Therefore, to constrain these additional possible background components, the higher energy data do have an effect, confirming that only the two levels at $E_x = 2.37$ and 3.50 MeV plus the external capture are needed to fit the experimental data up to the $E_x = 3.50$ MeV resonance. At higher energies, background components do become necessary to describe the data as given in Table III.

Asymptotic normalization coefficients (ANCs) provide a more model independent method of bridging the gap between the way bound state strengths are characterized using the coupled reaction channels formalism and R matrix [59]. The recent studies by Li *et al.* [35] and Artemov *et al.* [36] report the proton ANC for the ground state of ^{13}N to be 1.64(11) and 1.63(13) fm$^{-1/2}$, respectively, in excellent agreement with that found from the present R-matrix fit of 1.615(52) fm$^{-1/2}$.

Figure 11 shows the extrapolated S factor of the $^{12}C(p,\gamma)^{13}N$ reaction to low energy using the R-matrix fit described in Sec. V. Traditionally, the S factor is quoted at $E_{c.m.} = 25$ keV or $S(25$ keV$)$, and past extrapolated values are compared with that of the present work in Table IV. Despite the issues discussed here concerning past cross section normalizations, the extrapolated values of $S(25$ keV$)$ from different works have remained remarkably consistency. Of all the past works that quote values for $S(25$ keV$)$ only that of Li *et al.* [35] is more than 1σ outside the present

TABLE IV. Comparison of $S(25 \text{ keV})$ values.

Ref.	$S(25 \text{ keV})$ (keV b)
Hebbard and Vogl [29] (1960)	1.33 ± 0.15
Rolfs and Azuma [32] (1974)	1.45 ± 0.20
Barker and Ferdous [33] (1980)	1.54 ± 0.08
Burtebaev *et al.* [37] (2008)	1.75 ± 0.22
Azuma *et al.* [6] (2010)	1.61 ± 0.29
Li *et al.* [35] (2010)	1.87 ± 0.13
Artemov *et al.* [36] (2022)	1.72 ± 0.15
This work	1.48 ± 0.09

value. This consistency between different extrapolations is somewhat surprising, but is the result of similar estimates for the direct component of the cross section, which comes to dominate at low energies, despite 30% variation in the high energy resonant cross section data.

VII. REACTION RATE

Figure 12 compares the rates of the present work and those provided in Li *et al.* [35] and NACRE II [5], relative to that of the NACRE compilation [60], in order to highlight the differences. A reaction rate is shown graphically in Burtebaev *et al.* [37], but no table or equation was found to facilitate an accurate comparison. It is interesting to note that at low temperatures all of the reaction rates, except for that of Li *et al.* [35], converge to a very similar value. This reflects the dominance of the direct capture at these low temperatures, similar to the consistency observed in values of $S(25 \text{ keV})$ reported by previous works. At higher temperatures the resonance contributions become dominant, resulting in more deviations in the rate. In particular, the present rate is lower than that of NACRE [60], Li *et al.* [35], and NACRE2 [5]
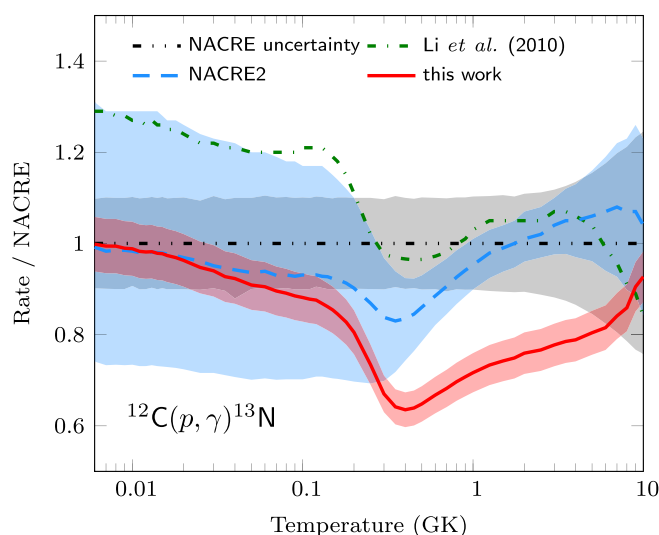

FIG. 12. Ratio of the rates for the $^{12}\text{C}(p, \gamma)^{13}\text{N}$ reaction for previous calculations by Li *et al.* [35] and NACRE II [5] and the present work to that of the NACRE compilation [60]. The uncertainty band of the present work corresponds to a 68% confidence interval.

at temperatures above ≈ 0.2 GK, reflecting the lower value in the cross section over the $E_p = 460$ keV resonance. It should be noted that while Barker and Ferdous [33], Hinds and Barker [34], and Azuma *et al.* [6] also adopted this lower cross section normalization, they did not propagate it to the reaction rate, thus the present work is the first to provide a rate reflecting this change. The tabulated rate is given in the Supplemental Material [42].

VIII. CONCLUSION

Solar neutrinos provide a window into the inner workings of our sun. These measurements have recently reached a level of sensitivity that allows them to distinguish neutrino fluxes from not only the dominant *pp*-chains but also the much weaker CNO cycle. In particular, neutrino fluxes from the β^+ decay of ^{15}O, coming from the $^{14}\text{N}(p, \gamma)^{15}\text{O}$ reaction, have been observed by BOREXINO for the first time. It therefore seems plausible that next generation detectors will be able to reach the sensitivity needed to observe the lower energy neutrinos from ^{13}N decay produced by the $^{12}\text{C}(p, \gamma)^{13}\text{N}$ reaction. To compare these neutrino flux measurements with solar model predictions, accurate cross sections are a main ingredient, with the largest sources of uncertainties now often coming from the cross sections. The reactions controlling early conversion of metals in the solar core and the approach to equilibrium are the $^{12}\text{C}(p, \gamma)^{13}\text{N}$ reaction analyzed here and the previously studied $^{14}\text{N}(p, \gamma)^{15}\text{O}$ reaction; these are the next-to-slowest and slowest rates in the lower temperature CN cycle, respectively. However, equilibrium for the CN cycles between production and depletion reactions is not completely established. As pointed out by Haxton and Serenelli [2], about 30% of the ^{13}N neutrinos come from the outer region of the solar core, where the CN cycle has not established the equilibrium stage, affecting the observed neutrino rate. A quantification of this effect would require a more detailed analysis of the burning conditions in the solar core within the framework of the standard solar model than can be done in this study.

In summary, for this study the $^{12}\text{C}(p, \gamma)^{13}\text{N}$ reaction has been reinvestigated with the goal of resolving past experimental discrepancies in both the absolute scale of the cross section and the energy calibration. To accomplish this, experimental measurements were made using both thin and thick targets and a discrepancy in the overall normalization in the cross section resulting from changes in the proton in carbon stopping powers from the 1950s to present day were found that result in an $\approx 30\%$ reduction in the overall resonance cross section. Further, the higher energy differential cross section data of this work placed additional constraints on possible background R-matrix components and shed light on an energy discrepancy present in Rolfs and Azuma [32]. Using an AZURE2 R matrix and BRICK Bayesian uncertainty analysis, and by comparing with thick-target yields, a more accurate and precise overall normalization of the data and low energy extrapolation of the S factor was obtained, resulting in an uncertainty in the rate of $\approx 6\%$. A updated reaction rate, that reflects these charges, has been presented.

[1] M. Agostini, K. Altenmüller, S. Appel, V. Atroshchenko, Z. Bagdasarian, D. Basilico, G. Bellini, J. Benziger, R. Biondi, D. Bravo, B. Caccianiga, F. Calaprice, A. Caminata, P. Cavalcante, A. Chepurnov, D. D'Angelo, S. Davini, A. Derbin, A. Di Giacinto, V. Di Marcello *et al.*, Experimental evidence of neutrinos produced in the CNO fusion cycle in the Sun, Nature (London) **587**, 577 (2020).

[2] W. C. Haxton and A. M. Serenelli, CN cycle solar neutrinos and the sun's primordial core metallicity, Astrophys. J. **687**, 678 (2008).

[3] A. Serenelli, C. Peña-Garay, and W. C. Haxton, Using the standard solar model to constrain solar composition and nuclear reaction *S* factors, Phys. Rev. D **87**, 043001 (2013).

[4] B. Frentz, A. Aprahamian, A. Boeltzig, T. Borgwardt, A. M. Clark, R. J. deBoer, G. Gilardy, J. Görres, M. Hanhardt, S. L. Henderson, K. B. Howard, T. Kadlecek, Q. Liu, K. T. Macon, S. Moylan, C. S. Reingold, D. Robertson, C. Seymour, S. Y. Strauss, F. Strieder, B. Vande Kolk, and M. Wiescher, Investigation of the ^{14}N(p, γ)^{15}O reaction and its impact on the CNO cycle, Phys. Rev. C **106**, 065803 (2022).

[5] Y. Xu, K. Takahashi, S. Goriely, M. Arnould, M. Ohta, and H. Utsunomiya, NACRE II: An update of the NACRE compilation of charged-particle-induced thermonuclear reaction rates for nuclei with mass number $A < 16$, Nucl. Phys. A **918**, 61 (2013).

[6] R. E. Azuma, E. Uberseder, E. C. Simpson, C. R. Brune, H. Costantini, R. J. de Boer, J. Görres, M. Heil, P. J. Leblanc, C. Ugalde, and M. Wiescher, AZURE: An *R*-matrix code for nuclear astrophysics, Phys. Rev. C **81**, 045805 (2010).

[7] Lugaro *et al.*, Annual Review of Nuclear and Particle Science (unpublished).

[8] O. Clarkson, F. Herwig, and M. Pignatari, Pop III *i*-process nucleosynthesis and the elemental abundances of SMSS J0313-6708 and the most iron-poor stars, Mon. Not. R. Astron. Soc. Lett. **474**, L37 (2018).

[9] K. J. Shen and L. Bildsten, Unstable helium shell burning on accreting white dwarfs, Astrophys. J. **699**, 1365 (2009).

[10] H. Y. Lee, M. Couder, A. Couture, S. Falahat, J. Görres, L. Lamm, P. J. LeBlanc, S. O'Brien, A. Palumbo, E. Stech, E. Strandberg, W. Tan, C. Ugalde, and M. Wiescher, Cross-section measurement of the ^{18}F(α, p)^{21}Ne reaction and possible implication for neutron production in explosive helium burning, Phys. Rev. C **80**, 025805 (2009).

[11] R. Pakmor, F. P. Callan, C. E. Collins, S. E. de Mink, A. Holas, W. E. Kerzendorf, M. Kromer, P. G. Neuneufel, J. T. O'Brien, F. K. Röpke, A. J. Ruiter, I. R. Seitenzahl, L. J. Shingles, S. A. Sim, and S. Taubenberger, On the fate of the secondary white dwarf in double-degenerate double-detonation Type Ia supernovae, Mon. Not. R. Astron. Soc. **517**, 5260 (2022).

[12] F. Joliot and I. Curie, Artificial production of a new kind radio-element, Nature (London) **133**, 201 (1934).

[13] *Nobel Lectures in Chemistry 1922–1941* (World Scientific, Singapore, 1999).

[14] C. Cockcroft, C. Gilbert, and E. Walton, Production of induced radioactivity by high velocity protons, Nature (London) **133**, 328 (1934).

[15] L. Hafstad and M. A. Tuve, Carbon radioactivity and other resonance transmutations by protons, Phys. Rev. **48**, 306 (1935).

[16] R. Roberts and N. Heydenburg, Further observations on the production of N^{13}, Phys. Rev. **53**, 374 (1938).

[17] S. C. Curran, P. I. Dee, and V. Petrzilka, The excitation of γ-radiation in processes of proton capture by light elements, Proc. R. Soc. London, Ser. A **169**, 269 (1938).

[18] R. Tangen, Experimental investigations of proton capture processes in light elements, Kgl. Norske Vid. Selsk. Skriften **1**, 1 (1946).

[19] F. Ajzenberg-Selove and T. Lauritsen, Energy levels of light nuclei VI, Nucl. Phys. **11**, 1 (1959).

[20] F. Ajzenberg-Selove, Energy levels of light-nuclei $A = 13$–15, Nucl. Phys. A **268**, 1 (1976).

[21] M. Wiescher, The history and impact of the CNO cycles in nuclear astrophysics, Phys. Perspect. **20**, 124 (2018).

[22] W. A. Fowler, C. C. Lauritsen, and T. Lauritsen, Gamma-radiation from excited states of light nuclei, Rev. Mod. Phys. **20**, 236 (1948).

[23] W. A. Fowler and C. C. Lauritsen, Gamma-radiation from light nuclei under proton bombardment, Phys. Rev. **76**, 314 (1949).

[24] J. D. Seagrave, The thick target yield of the reaction C$^{12}(p, \gamma)$N$^{13}(\beta^+)$C^{13}, Phys. Rev. **84**, 1219 (1951).

[25] J. D. Seagrave, Radiative capture of protons by C^{13}, Phys. Rev. **85**, 197 (1952).

[26] R. N. Hall and W. A. Fowler, The cross section for the radiative capture of protons by C^{12} near 100 keV, Phys. Rev. **77**, 197 (1950).

[27] C. L. Bailey and W. R. Stratton, Cross section of the C$^{12}(p, \gamma)$N^{13} reaction at low energies, Phys. Rev. **77**, 194 (1950).

[28] W. A. S. Lamb and R. E. Hester, Radiative capture of protons in carbon from 80 to 126 keV, Phys. Rev. **107**, 550 (1957).

[29] D. Hebbard and J. Vogl, Elastic scattering and radiative capture of protons by C^{13}, Nucl. Phys. **21**, 652 (1960).

[30] J. L. Vogl, Radiative capture of protons by C^{12} and C^{13} below 700 keV, Ph.D. thesis, California Institute of Technology, Pasadena, California, 1963 (unpublished).

[31] F. Young, J. Armstrong, and J. Marion, Interference effects in the C$^{12}(p, \gamma)$N^{13} reaction, Nucl. Phys. **44**, 486 (1963).

[32] C. Rolfs and R. Azuma, Interference effects in ^{12}C(p, γ)^{13}N and direct capture to unbound states, Nucl. Phys. A **227**, 291 (1974).

[33] F. Barker and N. Ferdous, The low-lying levels of ^{13}C and ^{13}N, Aust. J. Phys. **33**, 691 (1980).

[34] S. Hinds and F. C. Barker, The ^{12}C(p,γ)^{13}N cross section near the $E_p = 0.46$MeV peak, Aust. J. Phys. **45**, 749 (1992).

[35] Z. Li, J. Su, B. Guo, Z. Li, X. Bai, J. Liu, Y. Li, S. Yan, B. Wang, Y. Wang, G. Lian, S. Zeng, E. Li, Y. Chen, N. Shu, Q. Fan, and

W. Liu, Determination of the ^{12}C(p, γ)^{13}N reaction rates from the ^{12}C$(^{7}$Li, ^{6}He$)$^{13}N reaction, Sci. China Phys. Mech. Astron. **53**, 658 (2010).

[36] S. V. Artemov, R. Yarmukhamedov, N. Burtebayev, B. K. Karakozov, F. K. Ergashev, M. Nassurlla, S. B. Igamov, N. Amangeldi, A. Morzabayev, J. Burtebayeva, V. S. Zhdanov, G. Yergaliuly, E. Piasecki, K. Rusek, S. B. Sakuta, A. Demyanova, O. R. Tojiboev, A. Trzcińska, A. Sabidolda, R. Khojayev *et al.*, Asymptotic normalization coefficient for ^{12}C$+p \rightarrow$ ^{13}N from the ^{12}C$(^{10}$B, ^{9}Be$)$^{13}N reaction and the ^{12}C(p, γ)^{13}N astrophysical S factor, Eur. Phys. J. A **58**, 24 (2022).

[37] N. Burtebaev, S. B. Igamov, R. J. Peterson, R. Yarmukhamedov, and D. M. Zazulin, New measurements of the astrophysical s factor for ^{12}C(p, γ)^{13}N reaction at low energies and the asymptotic normalization coefficient (nuclear vertex constant) for the $p + {}^{12}$C $\rightarrow$ ^{13}N reaction, Phys. Rev. C **78**, 035802 (2008).

[38] H. Meyer, G. Plattner, and I. Sick, Elastic $p + {}^{12}$C scattering between 0.3 and 2 MeV, Z. Phys. A **279**, 41 (1976).

[39] A. Antilla, J. Keinonen, M. Hautala, and I. Forsblom, Use of the ^{27}Al(p, γ)^{28}Si, $E_p = 992$ keV resonance as a gamma-ray intensity standard, Nucl. Instrum. Methods **147**, 501 (1977).

[40] RUBION facility at the University of Bochum, https://www.rubion.rub.de/en/projects-in-rubion/.

[41] S. Daigle, K. J. Kelly, A. E. Champagne, M. Q. Buckner, C. Iliadis, and C. Howard, Measurement of the $E_r^{\text{c.m.}} = 259$keV resonance in the ^{14}N(p, γ)^{15}O reaction, Phys. Rev. C **94**, 025803 (2016).

[42] See Supplemental Material at http://link.aps.org/supplemental/10.1103/PhysRevC.108.035805 for the tabulated experimental data and reaction rate.

[43] M. E. Rose, The analysis of angular correlation and angular distribution data, Phys. Rev. **91**, 610 (1953).

[44] F. Ajzenberg-Selove, Energy levels of light nuclei $A = 13$–15, Nucl. Phys. A **523**, 1 (1991).

[45] M. Kokkoris, P. Misaelides, S. Kossionides, C. Zarkadas, A. Lagoyannis, R. Vlastou, C. Papadopoulos, and A. Kontos, A detailed study of the ^{12}C(d, p_0)^{13}C reaction at detector angles between 135° and 170°, for the energy range $E_{d,lab} = $ 900–2000 keV, Nucl. Instrum. Methods Phys. Res., Sect. B **249**, 77 (2006), special issue: Ion Beam Analysis.

[46] J. Pacheco de Carvalho and A. Reis, Differential cross-section measurements for the ^{12}C(d, p_0)^{13}C reaction and applications to surface analysis of materials, Nucl. Instrum. Methods Phys. Res., Sect. B **266**, 2263 (2008), special issue: Accelerators in Applied Research and Technology.

[47] G. Imbriani, H. Costantini, A. Formicola, A. Vomiero, C. Angulo, D. Bemmerer, R. Bonetti, C. Broggini, F. Confortola, P.

Corvisiero, J. Cruz, P. Descouvemont, Z. Fülöp, G. Gervino, A. Guglielmetti, C. Gustavino, G. Gyürky, A. P. Jesus, M. Junker, J. N. Klug *et al.*, S-factor of ^{14}N(p, γ)^{15}O at astrophysical energies, Eur. Phys. J. A **25**, 455 (2005).

[48] J. D. Seagrave, Radiative Capture of Protons by C^{12} and C^{13}, Ph.D. thesis, California Institute of Technology, 1951 (unpublished).

[49] J. F. Ziegler, M. D. Ziegler, and J. P. Biersack, SRIM - The stopping and range of ions in matter (2010), Nucl. Instrum. Methods Phys. Res., Sect. B **268**, 1818 (2010).

[50] E. Uberseder and R. J. deBoer, AZURE2 User Manual, 2015.

[51] C. R. Brune, Alternative parametrization of R-matrix theory, Phys. Rev. C **66**, 044611 (2002).

[52] W. Huang, G. Audi, M. Wang, F. G. Kondev, S. Naimi, and X. Xu, The AME2016 atomic mass evaluation (I). Evaluation of input data and adjustment procedures, Chin. Phys. C **41**, 030002 (2017).

[53] M. Wang, G. Audi, F. G. Kondev, W. Huang, S. Naimi, and X. Xu, The AME2016 atomic mass evaluation (II). Tables, graphs and references, Chin. Phys. C **41**, 030003 (2017).

[54] D. Odell, C. R. Brune, D. R. Phillips, R. J. deBoer, and S. N. Paneru, Performing Bayesian analyses with AZURE2 using BRICK: An application to the ^{7}Be system, Front. Phys. **10**, 888476 (2022).

[55] R. J. Holt, H. E. Jackson, R. M. Laszewski, J. E. Monahan, and J. R. Specht, Effects of channel and potential radiative transitions in the ^{17}O(γ, n_0)^{16}O reaction, Phys. Rev. C **18**, 1962 (1978).

[56] F. C. Barker and T. Kajino, The ^{12}C(α, γ)^{16}O cross section at low energies, Aust. J. Phys. **44**, 369 (1991).

[57] C. Angulo and P. Descouvemont, The ^{14}N(p, γ)^{15}O low-energy S-factor, Nucl. Phys. A **690**, 755 (2001).

[58] D. Foreman-Mackey, D. W. Hogg, D. Lang, and J. Goodman, emcee: The MCMC hammer, Publ. Astron. Soc. Pac. **125**, 306 (2013).

[59] R. E. Tribble, C. A. Bertulani, M. La Cognata, A. M. Mukhamedzhanov, and C. Spitaleri, Indirect techniques in nuclear astrophysics: A review, Rep. Prog. Phys. **77**, 106901 (2014).

[60] C. Angulo, M. Arnould, M. Rayet, P. Descouvemont, D. Baye, C. Leclercq-Willain, A. Coc, S. Barhoumi, P. Aguer, C. Rolfs, R. Kunz, J. Hammer, A. Mayer, T. Paradellis, S. Kossionides, C. Chronidou, K. Spyrou, S. Degl'Innocenti, G. Fiorentini, B. Ricci *et al.*, A compilation of charged-particle induced thermonuclear reaction rates, Nucl. Phys. A **656**, 3 (1999).